

---

# v1: Learning to Point Visual Tokens for Multimodal Mathematical Grounded Reasoning

---

Jiwan Chung<sup>\*1</sup> Junhyeok Kim<sup>\*1</sup> Siyeol Kim<sup>1</sup> Minsoo Kim<sup>1</sup> Jaeyoung Lee<sup>2</sup> Youngjae Yu<sup>2</sup>

## Abstract

When thinking with images, humans rarely rely on a single glance: they revisit visual evidence while reasoning. In contrast, most Multimodal Language Models encode an image once to key-value cache and then reason purely in text, making it hard to re-ground intermediate steps. We empirically confirm this: as reasoning chains lengthen, models progressively lose focus on relevant regions. We introduce **v1**, a lightweight extension for active visual referencing via point-and-copy: the model selects relevant image patches and copies their embeddings back into the reasoning stream. Crucially, our point-and-copy mechanism retrieves patches using their semantic representations as keys, ensuring perceptual evidence remains aligned with the reasoning space. To train this behavior, we build **v1g**, a dataset of 300K multimodal reasoning traces with interleaved grounding annotations. Across multimodal mathematical reasoning benchmarks, **v1** consistently outperforms comparable baselines. We plan to release the model checkpoint and data.

## 1. Introduction

Multimodal mathematical problem solving often requires repeated access to diagrams: intermediate steps depend on localized cues (e.g., angles, tangency points, symmetries) that are revisited as reasoning unfolds. Cognitive studies report similar visual revisitation (Cox, 1999; Brun et al., 2016; Chu et al., 2017; Kozhevnikov et al., 2002).

Recent advances in Multimodal Large Language Models (MLLMs) (Liu et al., 2023a; Bai et al., 2025; Chen et al., 2025) have shifted focus toward complex multi-step reasoning (Xu et al., 2025; Yao et al., 2024; Sun et al., 2025; Huang et al., 2025) rather than direct recognition. Mathematical reasoning (Lu et al., 2024; Zhang et al., 2024a; Wang et al.,

2024a) is a standard benchmark for this capability; its requirement for long-horizon grounding and unambiguous solutions provides a rigorous setting for studying grounded multimodal inference.

However, current MLLMs process images only once at the start and, due to causal masking, thereafter reason mainly over the frozen key-value cache of visual embeddings. This limits their ability to actively revisit visual context as inference unfolds. In practice, this constraint manifests as two forms of *visual grounding decay*. First, attention to all image tokens steadily weakens as reasoning chains extend. Second, even the relative weight on relevant tokens declines, reducing the model’s ability to focus on the most informative regions (Section 3). These effects highlight the need for mechanisms that let models explicitly re-access visual information to keep reasoning grounded in the input.

We propose **v1**, a simple yet effective extension that equips MLLMs with a *point-and-copy* mechanism for dynamically referencing input visual tokens during multimodal mathematical reasoning (Figure 1). Specifically, we augment the model with an additional pointing head that outputs a probability distribution over the input image token positions, alongside the standard vocabulary logits. When an image token is selected, its embedding is copied and injected as the next-step input, allowing the model to dynamically retrieve and reuse visual information during generation.

Our approach is readily compatible with popular MLLM architectures (Liu et al., 2023a; Wang et al., 2024c; Chen et al., 2025) that operate on continuous image embeddings. Unlike methods that attempt to generate new image tokens (Chameleon Team, 2024) which require full-scale pretraining for image generation capacity, our method simply reuses existing input embeddings through pointing and copying. The only additional parameters are lightweight linear heads, incurring minimal computational overhead.

To train **v1**, we construct **v1g**, a dataset of 300K multimodal mathematical reasoning paths with interleaved grounding annotations, where each reasoning step is explicitly linked to a corresponding image region. The construction pipeline comprises three stages: (1) oversampling diverse reasoning traces from an MLLM, (2) extracting visual queries and

<sup>1</sup>Yonsei University <sup>2</sup>Seoul National University. Correspondence to: Jiwan Chung <jiwan.chung.research@gmail.com>.

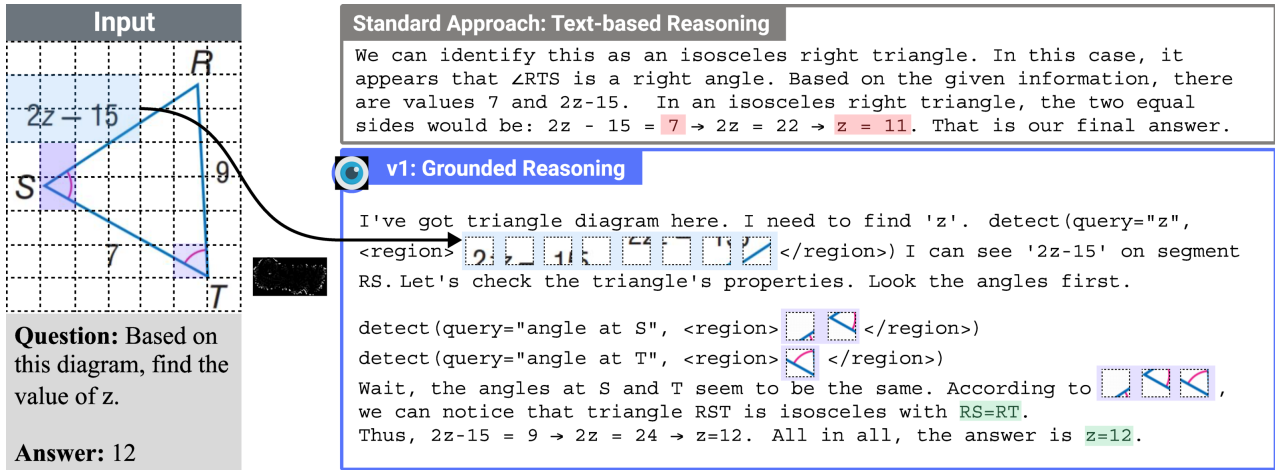


Figure 1. Pure text-based reasoning vs. v1 during inference. Our v1 can actively re-access visual context by pointing to and copying relevant image regions throughout the reasoning process.

retrieval steps from the traces using an LLM-guided decomposition process, and (3) grounding each visual reference by associating it with a bounding box in the input image. The pipeline is fully automated, leveraging the generative and interpretive capabilities of LLMs to produce high-quality, grounded reasoning trajectories at scale.

We evaluate v1 on three established multimodal mathematical reasoning benchmarks: MathVista (Lu et al., 2024), MathVision (Wang et al., 2024b), and MathVerse (Zhang et al., 2024a), following prior work (Yao et al., 2024; Sun et al., 2025; Huang et al., 2025). v1 demonstrates strong performance across all benchmarks, outperforming existing models of comparable scale and approaching the capabilities of much larger models, particularly on tasks requiring precise visual grounding and iterative reference to localized regions. These results suggest that dynamic access of visual input at inference time can improve multimodal mathematical reasoning capabilities.

Our contributions are:

- **v1 model:** a lightweight MLLM extension that helps mitigate visual grounding decay through a point-and-copy mechanism, enabling dynamic visual reference.
- **v1g dataset:** a large-scale training set with 300K multimodal mathematical reasoning traces and fine-grained visual grounding.
- **Empirical findings:** extensive experiments and ablations on multimodal mathematical reasoning benchmarks, showing that dynamic visual reference and the point-and-copy design both mitigate visual grounding decay and lead to better multimodal reasoning.

## 2. Related Work

### 2.1. Reasoning in Large Language Models

**Reasoning in text-only large language models.** Recent advances have significantly improved reasoning in text-only LLMs. OpenAI’s o1 model (Jaech et al., 2024) had achieved state-of-the-art performance on mathematical benchmarks (Lightman et al., 2023; Cobbe et al., 2021), motivating follow-up work that induces stronger reasoning through reinforcement learning and reflective Chain-of-Thought (Guo et al., 2025), as well as inference-time scaling (Muennighoff et al., 2025). While effective in text-only settings, extending these approaches to multimodal reasoning remains challenging.

**Reasoning in multimodal large language models.** Multimodal reasoning poses challenges beyond text-only inference, requiring both visual perception and the integration of visual inputs into multi-step reasoning. Early approaches (Liu et al., 2023a; Chen et al., 2024; Zhang et al., 2024b; Yang et al., 2023) typically convert images into textual descriptions for downstream tasks. More recently, inspired by Chain-of-Thought prompting in LLMs, models such as LLaVA-CoT (Xu et al., 2025), TVC (Sun et al., 2025), and Mulberry (Yao et al., 2024), among others (Huang et al., 2025; Deng et al., 2025; Meng et al., 2025; Wu et al., 2025; Wang et al., 2025), extend CoT reasoning to multimodal settings and achieve strong results on benchmarks such as MathVista (Lu et al., 2024) and MathVision (Wang et al., 2024b). However, these models treat visual inputs as fixed context and perform reasoning entirely in the text space, lacking explicit mechanisms to re-access or ground their reasoning in visual representations.

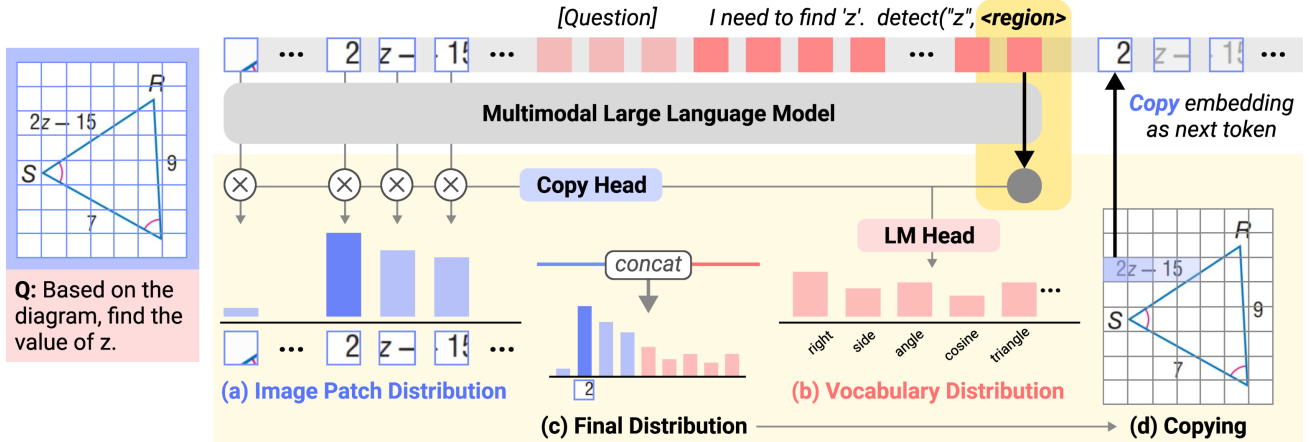


Figure 2. **Inference process of  $v1$ .** At each step, the MLLM encodes the multimodal context and generation history into token representations. For the last token (e.g., " $\langle region \rangle$ "), (a) a copy head projects its representation and computes logits against image patch embeddings, (b) a language head produces logits over the vocabulary, and (c) the two are concatenated to form the final distribution. If a patch is chosen, its embedding is copied as the next token input, enabling  $v1$  to reference image regions one patch at a time.

## 2.2. Implementing Visual Reference

A growing body of work equips MLLMs with mechanisms to interact with images more explicitly during reasoning, beyond treating the visual input as a single, static context. Existing approaches span a range of design choices, including predicting structured spatial references (e.g., boxes or points) to retrieve localized evidence (Gupta & Kembhavi, 2023; Wu & Xie, 2023; Chung et al., 2025; Jiang et al., 2025), generating intermediate visual artifacts (e.g., sketches or diagrams) to externalize intermediate states (Hu et al., 2024; Borzjanizadeh et al., 2025; Li et al., 2025; Ma et al., 2025), and hybrid tool-use pipelines that interleave perception and reasoning steps (Gupta & Kembhavi, 2023; Hu et al., 2024).

Our work is most closely related to methods that enable *visual re-access* during decoding. We extend the pointer-generator idea (See et al., 2017) from selective copying in text to selectively reusing visual token embeddings, yielding an interpretable and lightweight mechanism to incorporate image evidence without emitting explicit coordinates or invoking image synthesis.

## 3. Visual Grounding Decays During Reasoning

To examine how visual attention evolves at each generation step, we use RefCOCO (Kazemzadeh et al., 2014), a visual reference expression generation benchmark where the task is to create a caption that uniquely identifies a target region specified by a bounding box. Although RefCOCO generally involves shorter generations than mathematical reasoning, it provides a controlled setting for measuring attention dynamics over visual regions. We analyze the TVC-7B model (Sun et al., 2025) on the RefCOCO testA

split, examining attention from the most recent token to all image tokens across early, middle, and late transformer layers (layers 2, 14, and 27).

The first analysis (Figure 3) tracks total attention to image tokens and shows a steady decline across decoding steps, indicating a reduced reliance on visual grounding as generation proceeds. The second analysis (Figure 4) measures attention to the target region by computing the ratio of mean attention on bounding-box image tokens to that over all image tokens. While layers 14 and 27 initially place greater emphasis on the target region, attention converges to a ratio of  $\sim 0.8$  by mid-generation, suggesting weakened relative focus on salient visual tokens.

These results suggest *visual grounding decay*, where attention to relevant visual content diminishes during extended generation. This limitation is especially relevant for multimodal reasoning tasks, such as mathematics, where intermediate steps may benefit from revisiting visual evidence, thereby motivating architectures with dynamic visual access during inference.

## 4. Method

At inference time,  $v1$  operates as a single, self-contained MLLM: all textual reasoning, visual localization, and point-and-copy operations are performed by the same fine-tuned backbone without invoking external models or tools.

### 4.1. Preliminary: Pointing for Language Generation

**Formulation.** We formulate a conditional next-token prediction objective, as commonly adopted in modern multimodal large language models (MLLMs). Given a sequence of continuous input representations  $c$  (e.g. embedded text

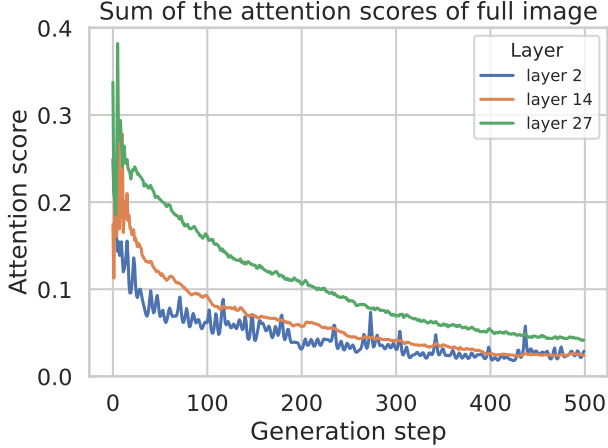


Figure 3. **Cumulative attention across all visual tokens**, showing a gradual decrease in overall attention to the input image tokens.

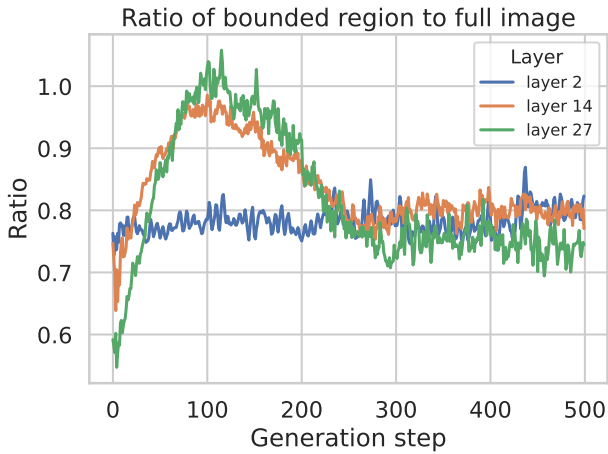


Figure 4. **Attention dynamics during reasoning**, showing that semantically important visual regions receive disproportionately low attention, suggesting inefficient grounding during reasoning.

tokens or visual features) the model is trained to autoregressively predict the discrete next token  $x_t$  conditioned on the input  $c$  and previously generated tokens  $x_{<t}$ :

$$p(x_1, \dots, x_T | c) = \prod_{t=1}^T p(x_t | c, x_1, \dots, x_{t-1})$$

The continuous input sequence  $c$  may include a heterogeneous mixture of modality-specific features, such as embedded discrete text tokens or continuous visual embeddings produced by image encoders (e.g. CLIP (Radford et al., 2021)). This general formulation covers a wide range of multimodal architectures such as LLaVA (Liu et al., 2023a) and Qwen-VL (Bai et al., 2025), which use continuous input image representations.

**Pointing.** For visually grounded reasoning, rather than generating new visual tokens, we instead teach the models to *point* to its position within the input image sequence it already understands, thereby referencing it explicitly.

The pointing mechanism we examine was first introduced by the pointer-generator network (See et al., 2017) in text summarization research. In the pointer-generator network, the input context sequence  $c$  also consists of discrete tokens within the vocabulary space  $V$ , unlike our setup. The model dynamically mixes two distributions at each decoding step  $t$ : (1) a generation distribution over the vocabulary  $P_{\text{gen}}(x_t)$ , and (2) a copy distribution  $P_{\text{ptr}}(x_t)$  over input tokens. The final output probability is given by a gated mixture:

$$p(x_t | c, x_{<t}) = \lambda_t P_{\text{gen}}(x_t) + (1 - \lambda_t) P_{\text{ptr}}(x_t), \quad (1)$$

$$\lambda_t \equiv \lambda(x_t | c, x_{<t}),$$

where  $\lambda \in [0, 1]$  is a learnable scalar gate that controls the trade-off between generating a new token and copying one from the input.

The pointer distribution is obtained via attention over the encoder representations:

$$\alpha_t^{(k)} = \frac{\exp(\text{score}(h_t, c_k))}{\sum_{k'} \exp(\text{score}(h_t, c_{k'}))}, \quad (2)$$

$$P_{\text{ptr}}(x_t = w) = \sum_{k: w_k = w} \alpha_t^{(k)}.$$

where  $h_t$  is the decoder hidden state at step  $t$ ,  $w_k$  the token at position  $k$ , and  $\text{score}$  denotes a standard attention scoring function (e.g., dot-product or additive). We generalized the formulation beyond the original implementation to arbitrary autoregressive language models for explanation purposes.

**Discrete targets.** The above formulation constrains the pointing targets to be within the discrete vocabulary space  $V$ . This prevents application to general MLLMs as the multimodal inputs often consist of continuous feature sequences (Liu et al., 2023a; Bai et al., 2025).

#### 4.2. v1: Pointing for Multimodal Grounded Reasoning

To overcome these limitations, we introduce **v1**, a lightweight extension to autoregressive MLLMs that enables explicit visual grounding by pointing to continuous input embeddings. **v1** augments the vocabulary with pointer tokens that allow the model to either generate text or copy visual content during inference. All reasoning and grounding are handled within a single fine-tuned backbone (e.g., Qwen-2.5-VL), without external modules or auxiliary grounding networks. This design supports unified inference over discrete and continuous modalities without modifying the core architecture (Figure 2).

**Pointing to continuous inputs.** The gated mixture formulation of (See et al., 2017) is not directly applicable to continuous inputs as image embeddings, as such inputs lack discrete mappings to vocabulary tokens  $V$ . To enable pointing in this setting, we extend the output space to include references to positions in the continuous input. Specifically, we define the augmented output space as  $\bar{V} = V \cup C$ , where  $C = \{c_1, c_2, \dots, c_K\}$  denotes the set of continuous input vectors (e.g. embeddings of the input image patches). This formulation allows the model to generate either a vocabulary token or a pointer to a specific continuous input. We denote a pointer to input vector  $c_k$  as  $\langle \text{ptr} : c_k \rangle$ , which is treated as a discrete token during decoding.

At each decoding step  $t$ , the model computes two distributions: (1) a generation distribution over the vocabulary  $V$ , producing logits  $\text{logit}_{\text{gen}} \in \mathbb{R}^{|V|}$ , and (2) a pointing distribution over the input positions  $C$ , producing logits  $\text{logit}_{\text{ptr}} \in \mathbb{R}^K$ . The final output logits are defined as:

$$\text{logit}_t = \left[ \text{logit}_{\text{gen}} \parallel \text{logit}_{\text{ptr}} \right] \in \mathbb{R}^{|V|+K}$$

where  $[\cdot \parallel \cdot]$  denotes concatenation. Pointing logits are computed by attending over the input sequence:

$$\text{logit}_{\text{ptr}}^{(k)} = \frac{L_q(h_t) \cdot L_k(c_k)^\top}{\sqrt{D}}$$

where  $h_t$  is the decoder hidden state at step  $t$ ,  $L_q$  and  $L_k$  are learned linear projections, and the scaling factor  $\sqrt{D}$  follows standard attention practice. We omit the gating module  $\lambda$  used in previous work, as the logit types are defined over disjoint spaces and do not require interpolation.

During inference, if the model selects an index in  $V$ , the next token  $x_t$  is emitted as the corresponding vocabulary token. If the model selects an index  $k \in C$ , the token is represented as a pointer  $x_t = \langle \text{ptr} : c_k \rangle$ . On the subsequent decoding step, the input embedding at position  $t$  is replaced with the continuous vector  $c_k$ , enabling the model to attend directly to the referenced content.

### 4.3. Annotating Visually-grounded Reasoning Data

To train **v1**, we require fine-grained multimodal reasoning traces in which each step is grounded to specific visual evidence. To this end, we construct **v1g**, a dataset of 300K multimodal reasoning paths with interleaved grounding annotations. Each trajectory includes a sequence of reasoning steps, where textual inferences are explicitly linked to corresponding image regions.

We generate the dataset using a fully automated three-stage pipeline: (1) oversampling textual reasoning paths from a pretrained MLLM, (2) decomposing each path into discrete visual queries and retrieval steps via an LLM, and (3)

grounding each visual reference by aligning it with a bounding box in the input image (see Section C and Figure 7 for details).

**Constructing base reasoning traces.** As a seed to our grounded corpus, we adopt the training set of TVC (Sun et al., 2025), which consists of reasoning traces generated from the QvQ model (Qwen Team, 2024). The dataset encompasses nine distinct problem domains: Charts, Documents, Geometry, IQ Tests, Medical Imagery, Natural Scenes, Science Diagrams, Synthetic Images, and Tables.

### Decomposing reasoning traces into visual reference steps.

We extract visual grounding cues from text-based reasoning traces using a strong off-the-shelf LLM (Gemini-2.0-flash (Google, 2025)). The model rewrites each reference to visual content as a *detect* call, which takes a short natural language description and returns the corresponding image region. Retrieved objects are cached and assigned symbolic identifiers  $\langle \text{obj}j\text{x} \rangle$  in order of appearance. In addition, the LLM generates a key-value list of visual components, with each key serving as a unique, descriptive grounding reference for later steps. We construct domain-specific few-shot prompts to guide this process, with prompt templates detailed in the Appendix. Finally, we post-process the LLM outputs to discard failure cases, including mismatches between referenced and retrieved objects, non-unique object labels, insufficient object count ( $\leq 2$ ), and ill-formed reasoning. After filtering,  $\sim 82\%$  samples are retained.

**Grounding visual references to image regions.** Visual grounding is challenging in multimodal reasoning tasks, since they often involve detecting abstract or unconventional regions (e.g. charts, geometry, medical scans). Existing grounding models perform poorly on such inputs (Steiner et al., 2024; Xiao et al., 2024). Moreover, these tasks frequently require grounding abstract or symbolic cues (e.g. angle ABC), which lie outside the training scope of current models.

To exploit the implicit visual grounding behavior in MLLMs, we build on Qwen2.5-VL’s visual grounding capacity (Bai et al., 2025). However, rather than relying on its coordinate generation interface, we estimate the model’s visual focus using a relative attention mechanism inspired by (Zhang et al., 2025), in order to better handle non-natural domains and symbolic cues. The corresponding algorithm is detailed in Appendix E. This produces a curated training set of  $\sim 300\text{K}$  grounded examples.

## 5. Implementation Details

**Preprocessing.** Given a multimodal input consisting of interleaved images, text, and bounding box annotations for

Table 1. Results on multimodal mathematical reasoning tasks. MathVision results are both reported for the mini and full subsets to include more baseline scores.

Model	Size	Reasoning Only	MathVista	MathVision	MathVerse	Average		
			mini	mini	full	mini	full	
Qwen2-VL (Wang et al., 2024c)	7B	✗	60.9	-	16.3	24.6	-	20.5
Qwen2-VL (Wang et al., 2024c)	72B	✗	69.7	-	26.6	36.2	-	31.4
Qwen2.5-VL (Bai et al., 2025)	7B	✗	67.8	23.6	-	44.5	45.3	-
Qwen2.5-VL (Bai et al., 2025)	72B	✗	74.8	39.8	-	57.6	57.4	-
InternVL2.5 (Chen et al., 2025)	8B	✗	64.4	22.0	19.7	39.5	41.9	29.6
InternVL2.5 (Chen et al., 2025)	78B	✗	72.3	34.9	32.2	51.7	53.0	42.0
GPT-4o (Hurst et al., 2024)	-	✗	63.8	-	30.4	50.2	-	40.3
LLaVa-CoT (Xu et al., 2025)	11B	✓	54.8	16.3	-	33.9	35.0	-
Mulberry (Yao et al., 2024)	7B	✓	63.1	-	-	39.6	-	-
TVC (Sun et al., 2025)	7B	✓	68.1	-	22.7	38.9	-	30.8
TVC (Sun et al., 2025)	72B	✓	72.2	-	41.9	48.8	-	45.4
QVQ-72B-preview (Qwen Team, 2024)	72B	✓	71.4	35.9	-	41.5	49.6	-
Base (Qwen2.5-VL)	7B	✗	67.8	23.6	-	44.5	45.3	-
Text-Only (TVC)	7B	✓	68.1	-	22.7	38.9	-	30.8
<b>Ours</b>	7B	✓	<b>68.6</b>	<b>34.5</b>	<b>28.1</b>	<b>48.6</b>	<b>50.6</b>	<b>38.4</b>
↳ Inference w/o Pointing	7B	✓	60.0	25.3	23.7	33.6	39.6	28.7

visual references, we first convert each image into a flattened sequence of image patches, following the patchification protocol used by the backbone model (e.g., Qwen2.5-VL (Bai et al., 2025)). Each bounding box is then transformed into a corresponding sequence of pointer tokens (e.g., <ptr4>, ..., <ptr32>), where each token refers to an enclosed image patch. These pointer tokens are appended to the tokenizer vocabulary but do not modify the model’s original embedding table or generation head. During preprocessing, the embeddings for pointer tokens are replaced with the corresponding image patch embeddings prior to the transformer layers. The final input is thus a unified sequence of text tokens, pointer tokens, and image patch embeddings.

**Model.** In this paper, we instantiate **v1** with Qwen-2.5-VL as MLLM backbone. Architecturally, we introduce only two lightweight linear layers atop the original model: a pointing query head  $L_q \in \mathbb{R}^{D \times D}$  and a pointing key head  $L_k \in \mathbb{R}^{D \times D}$ , where  $D$  denotes the latent dimensionality of the MLLM. Both heads are initialized as identity matrices scaled by  $1/\sqrt{D}$ , ensuring that their influence on the model’s initial output distribution remains minimal. This initialization strategy is particularly effective given the structure of our task: the pretrained backbone already produces meaningful generative likelihoods  $P_{\text{gen}}$ , and the pointing mechanism selects at most a single position per timestep from the pointing distribution  $P_{\text{ptr}}$ . As a result, the added modules integrate smoothly during early training and do not induce catastrophic forgetting.

**Training.** Given the dual-nature output space comprising a generative vocabulary  $V$  and a pointing reference set  $K$ , we incorporate z-loss regularization to stabilize the softmax partition function, following (Chowdhery et al., 2023; Wortsman et al., 2023; Chameleon Team, 2024). Specifically, we regularize the log-partition function  $Z = \sum_j e^{x_j}$  in the softmax  $\sigma(x)_i = e^{x_i}/Z$  by introducing a z-loss term  $\mathcal{L}_z = \lambda \log Z$ , where  $\lambda = 10^{-5}$ . To reduce computational overhead, we approximate  $Z$  using a top- $k = 40$  partition function  $\tilde{Z} = \sum_{j \in \text{TopK}(x)} e^{x_j}$ . This approximation enables efficient and numerically stable training in large-output-space settings. Further details are in Section A.

**Inference.** At each decoding step to generate token  $x_t$ , **v1** utilizes two additional caches: (1) keys, given by hidden features  $L_k(c)$  corresponding to image patch positions for computing the pointing logits  $\text{logit}_{\text{ptr}}$ , and (2) values, the input feature sequences of the associated image patches. These are essential for enabling the pointing and copying mechanism during inference. We implement the additional caches by extending the key-value attention caching interface of the HuggingFace (Wolf et al., 2020) Transformers library. The memory overhead is minimal compared to the standard attention cache, since we store only a small subset of the tokens (and only for a single layer) needed for point-and-copy.

The additional architectural cost of **v1** is minimal: we introduce a single linear projection applied to image embeddings (e.g., 256 tokens for a  $448 \times 448$  input), which is negligible compared to the vocabulary projection in the language head.

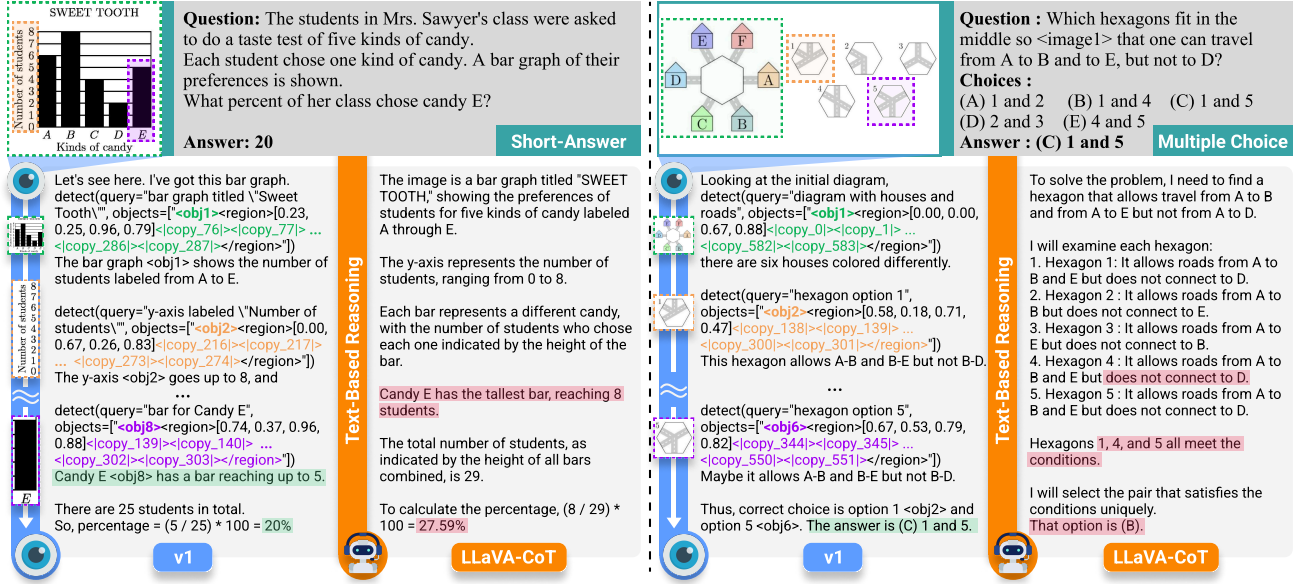


Figure 5. Qualitative comparison on MathVision. v1’s dynamic grounding helps to solve both bar graph and spatial reasoning tasks, while LLaVA-CoT misinterprets visual content in both cases.

Table 2. Ablation on MathVision testmini. All variants share the same backbone. Train denotes grounded-reasoning training, and Infer denotes enabling point-and-copy at inference.  $\Delta$  is measured relative to the backbone.

Variant	Tr.	Inf.	Score	$\Delta$
Backbone	✗	✗	23.6	–
Ours (no pointing)	✓	✗	25.3	+1.7
Ours	✓	✓	34.5	+10.9

During inference, point-and-copy increases sequence length by re-inserting visual tokens; in practice, copied visual tokens rarely exceed 60% of the textual token count due to revisit suppression, resulting in an average total sequence length of approximately 1.6 $\times$  that of text-only reasoning. No external models or executors are invoked, and all computation remains within a single autoregressive forward pass.

## 6. Experiments

### 6.1. Downstream Evaluation

**Setup.** We use three representative multimodal mathematical reasoning benchmarks: MathVista (mini) (Lu et al., 2024), MathVision (mini/full) (Wang et al., 2024b), and MathVerse (mini) (Zhang et al., 2024a). Following prior work (Duan et al., 2024), we use LLM to compare numerical answers for equations of different format for computing accuracy (Liu et al., 2023b).

We compare our method against both general-purpose and

reasoning-specialized MLLMs. General MLLMs include Qwen2-VL (Wang et al., 2024c) and Qwen2.5-VL (Bai et al., 2025) at both 7B and 72B scales, as well as InternVL2.5 (Chen et al., 2025) at 8B and 78B. We also include GPT-4o (Hurst et al., 2024) as a high-performing proprietary baseline. For reasoning-oriented models, we evaluate LLaVa-CoT-11B (Xu et al., 2025), Mulberry-7B (Yao et al., 2024), TVC-7B and 72B (Sun et al., 2025), and QVQ-72B-preview (Qwen Team, 2024).

**Results.** Quantitative results are presented in Table 1. Our approach yields substantial performance improvements over baseline models. Among 7B-scale models, v1 with full pointing capability outperforms both general-purpose and reasoning-specialized baselines. Notably, despite its smaller size, our 7B model narrows the performance gap with several 72B-scale models. The gains are particularly pronounced on MathVision, a benchmark known for its stronger demand for correct grounding.

### 6.2. Further Analysis

**Qualitative results.** Figure 5 compares our method with LLaVA-CoT (Xu et al., 2025) on MathVision short-answer and multiple-choice examples. Our v1 exhibits explicit visual grounding via pointer-based detection and selective copying of relevant image regions. In the bar graph example, v1 correctly identifies the bar for Candy E and computes the correct percentage, while LLaVA-CoT misidentifies the tallest bar. In the hexagon pathfinding task, v1 reasons over spatial connectivity by attending to structural differences among options, whereas LLaVA-CoT fails to eliminate in-

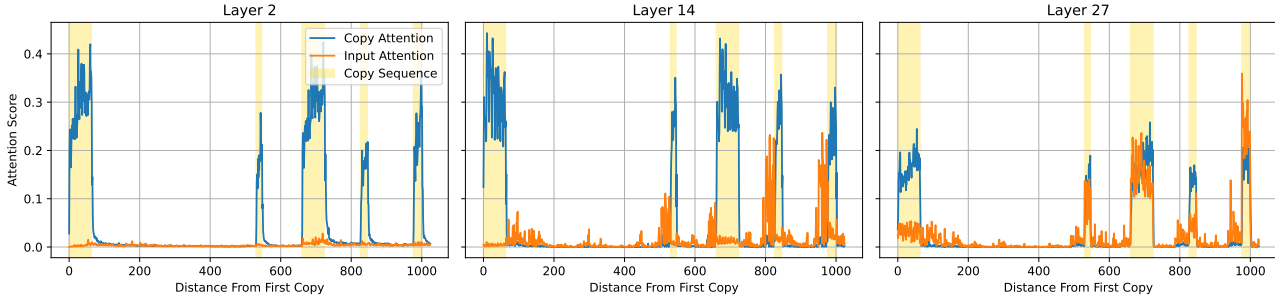


Figure 6. Comparison of attention to copy tokens vs. original visual tokens. Layer-wise sum of attention scores directed to copy tokens and their corresponding original visual input tokens from a **v1** output on a MathVision example. Copy token intervals are highlighted in yellow.

valid candidates. These examples illustrate how active visual reference supports more precise and interpretable grounded reasoning than text-only chain-of-thought methods.

**Ablation study.** We report an ablation study in Table 2 to isolate the effect of the point-and-copy mechanism. All variants share the same Qwen2.5-VL-7B backbone: *Backbone* applies no task-specific fine-tuning, while *Ours (no pointing)* uses the same training setup as **v1** but disables pointing at inference. On MathVision (testmini), **v1** improves over the backbone from 23.6 to 34.5 (+10.9), whereas disabling pointing reduces the score to 25.3 (+1.7), indicating that point-and-copy at inference is a key driver of the gains.

For context, TVC (Sun et al., 2025) serves as a text-only reasoning baseline; our training data extends its reasoning traces with additional visual-grounding annotations.

**How does **v1** utilize pointed visual regions?** We analyze how **v1** internally uses the visual regions retrieved via the point-and-copy mechanism. As shown in Figure 6, we compare the total *Input Attention* (attention to the original visual tokens) and *Copy Attention* (attention to the copied tokens) during generation after the first copy operation.

**How does **v1** utilize pointed visual regions?** We analyze how **v1** uses visual regions retrieved via the point-and-copy mechanism. As shown in Figure 6, we compare *Input Attention* (to original visual tokens) and *Copy Attention* (to copied tokens) during generation after the first copy operation.

We observe a structured sequence of behaviors. Before copying, attention to original image tokens increases, indicating a localization step in which relevant regions are identified. Immediately after copying, intermediate layers (e.g., layers 2 and 14) exhibit dominant copy attention, reflecting focused post-retrieval processing of the retrieved region. When averaged across layers, copied tokens consistently receive higher attention than original image tokens,

suggesting that copied regions serve as stable and accessible references. In higher layers (e.g., layer 27), attention to input and copied tokens becomes more balanced, which may correspond to a late-stage integration of retrieved visual information into the broader reasoning context.

Overall, these results indicate that **v1** exploits pointed visual regions through a progression from localization to focused processing and high-level integration.

## 7. Conclusion

We introduced **v1**, a lightweight extension that enables MLLMs to actively revisit input images via a point-and-copy mechanism, and **v1g**, a dataset of 300K multimodal reasoning traces with fine-grained visual grounding. Experiments on established multimodal mathematical reasoning benchmarks show that **v1** improves performance, particularly on tasks requiring grounded, multi-step visual reasoning. We hope this work encourages further exploration of dynamic visual access as a core component of multimodal reasoning.

## Impact Statement

This paper introduces **v1** framework, which allows MLLMs to explicitly re-access and reuse visual tokens during mathematical reasoning. The technique may improve accessibility and productivity in education and scientific practice by supporting clearer, more verifiable solutions grounded in figures and diagrams.

Risks are similar to those of other multimodal generative models: outputs can still be incorrect or overconfident; performance may vary across visual styles, domains, or languages; and improved figure understanding could facilitate misuse (e.g., generating plausible-but-wrong technical content or enabling academic dishonesty).

We encourage responsible use with human verification,

transparent reporting of limitations and failure modes, and avoiding deployment in high-stakes decision pipelines without rigorous validation and safeguards.

## References

- Bai, S., Chen, K., Liu, X., Wang, J., Ge, W., Song, S., Dang, K., Wang, P., Wang, S., Tang, J., Zhong, H., Zhu, Y., Yang, M., Li, Z., Wan, J., Wang, P., Ding, W., Fu, Z., Xu, Y., Ye, J., Zhang, X., Xie, T., Cheng, Z., Zhang, H., Yang, Z., Xu, H., and Lin, J. Qwen2.5-vl technical report, 2025. URL <https://arxiv.org/abs/2502.13923>.
- Borazjanizadeh, N., Herzig, R., Oks, E., Darrell, T., Feris, R., and Karlinsky, L. Visualizing thought: Conceptual diagrams enable robust planning in llms, 2025. URL <https://arxiv.org/abs/2503.11790>.
- Brun, J., Masson, P. L., and Weil, B. Designing with sketches: the generative effects of knowledge preordering. *Design Science*, 2, 2016. URL <https://api.semanticscholar.org/CorpusID:17302973>.
- Chameleon Team. Chameleon: Mixed-modal early-fusion foundation models. *arXiv preprint arXiv:2405.09818*, 2024.
- Chen, B., Xu, Z., Kirmani, S., Ichter, B., Sadigh, D., Guibas, L., and Xia, F. Spatialvlm: Endowing vision-language models with spatial reasoning capabilities. In *Proceedings of the IEEE/CVF Conference on Computer Vision and Pattern Recognition (CVPR)*, pp. 14455–14465, June 2024.
- Chen, Z., Wang, W., Cao, Y., Liu, Y., Gao, Z., Cui, E., Zhu, J., Ye, S., Tian, H., Liu, Z., Gu, L., Wang, X., Li, Q., Ren, Y., Chen, Z., Luo, J., Wang, J., Jiang, T., Wang, B., He, C., Shi, B., Zhang, X., Lv, H., Wang, Y., Shao, W., Chu, P., Tu, Z., He, T., Wu, Z., Deng, H., Ge, J., Chen, K., Zhang, K., Wang, L., Dou, M., Lu, L., Zhu, X., Lu, T., Lin, D., Qiao, Y., Dai, J., and Wang, W. Expanding performance boundaries of open-source multimodal models with model, data, and test-time scaling, 2025. URL <https://arxiv.org/abs/2412.05271>.
- Chowdhery, A., Narang, S., Devlin, J., Bosma, M., Mishra, G., Roberts, A., Barham, P., Chung, H. W., Sutton, C., Gehrmann, S., et al. Palm: Scaling language modeling with pathways. *Journal of Machine Learning Research*, 24(240):1–113, 2023.
- Chu, J., Fyfe, E. R., and Rittle-Johnson, B. Diagrams benefit symbolic problem-solving. *British Journal of Educational Psychology*, 87:273–287, 2017. URL <https://api.semanticscholar.org/CorpusID:14563301>.
- Chung, J., Kim, S., Jo, Y., Park, J., Min, D., and Yu, Y. Teaching metric distance to discrete autoregressive language models, 2025. URL <https://arxiv.org/abs/2503.02379>.
- Cobbe, K., Kosaraju, V., Bavarian, M., Chen, M., Jun, H., Kaiser, L., Plappert, M., Tworek, J., Hilton, J., Nakano, R., Hesse, C., and Schulman, J. Training verifiers to solve math word problems. *arXiv preprint arXiv:2110.14168*, 2021.
- Cox, R. J. Representation construction, externalised cognition and individual differences. *Learning and Instruction*, 9:343–363, 1999. URL <https://api.semanticscholar.org/CorpusID:143780266>.
- Deng, Y., Bansal, H., Yin, F., Peng, N., Wang, W., and Chang, K.-W. Opencilthinker: An early exploration to complex vision-language reasoning via iterative self-improvement, 2025. URL <https://arxiv.org/abs/2503.17352>.
- Duan, H., Yang, J., Qiao, Y., Fang, X., Chen, L., Liu, Y., Dong, X., Zang, Y., Zhang, P., Wang, J., et al. Vlmevalkit: An open-source toolkit for evaluating large multi-modality models. In *Proceedings of the 32nd ACM International Conference on Multimedia*, pp. 11198–11201, 2024.
- Google. Gemini 2.0 flash (gemini-2.0-flash-001), February 2025. URL <https://cloud.google.com/vertex-ai/generative-ai/docs/models/gemini/2-0-flash>.
- Guo, D., Yang, D., Zhang, H., Song, J., Zhang, R., Xu, R., Zhu, Q., Ma, S., Wang, P., Bi, X., et al. Deepseek-r1: Incentivizing reasoning capability in llms via reinforcement learning. *arXiv preprint arXiv:2501.12948*, 2025.
- Gupta, T. and Kembhavi, A. Visual programming: Compositional visual reasoning without training. In *Proceedings of the IEEE/CVF Conference on Computer Vision and Pattern Recognition (CVPR)*, pp. 14953–14962, June 2023.
- Hu, Y., Shi, W., Fu, X., Roth, D., Ostendorf, M., Zettlemoyer, L., Smith, N. A., and Krishna, R. Visual sketchpad: Sketching as a visual chain of thought for multimodal language models. In *The Thirty-eighth Annual Conference on Neural Information Processing Systems*, 2024. URL <https://openreview.net/forum?id=GNSM11P5VR>.
- Huang, W., Jia, B., Zhai, Z., Cao, S., Ye, Z., Zhao, F., Xu, Z., Hu, Y., and Lin, S. Vision-r1: Incentivizing reasoning capability in multimodal large language models, 2025. URL <https://arxiv.org/abs/2503.06749>.

- Hurst, A., Lerer, A., Goucher, A. P., Perelman, A., Ramesh, A., Clark, A., Ostrow, A., Welihinda, A., Hayes, A., Radford, A., et al. Gpt-4o system card. *arXiv preprint arXiv:2410.21276*, 2024.
- Jaech, A., Kalai, A., Lerer, A., Richardson, A., El-Kishky, A., Low, A., Helyar, A., Madry, A., Beutel, A., Carney, A., et al. Openai o1 system card. *arXiv preprint arXiv:2412.16720*, 2024.
- Jiang, Q., Huo, J., Chen, X., Xiong, Y., Zeng, Z., Chen, Y., Ren, T., Yu, J., and Zhang, L. Detect anything via next point prediction, 2025. URL <https://arxiv.org/abs/2510.12798>.
- Kazemzadeh, S., Ordonez, V., Matten, M., and Berg, T. ReferItGame: Referring to objects in photographs of natural scenes. In Moschitti, A., Pang, B., and Daelemans, W. (eds.), *Proceedings of the 2014 Conference on Empirical Methods in Natural Language Processing (EMNLP)*, pp. 787–798, Doha, Qatar, October 2014. Association for Computational Linguistics. doi: 10.3115/v1/D14-1086. URL <https://aclanthology.org/D14-1086>.
- Kozhevnikov, M., Hegarty, M., and and, R. E. M. Revising the visualizer-verbalizer dimension: Evidence for two types of visualizers. *Cognition and Instruction*, 20(1):47–77, 2002. doi: 10.1207/S1532690XCI2001\3. URL [https://doi.org/10.1207/S1532690XCI2001\\_3](https://doi.org/10.1207/S1532690XCI2001_3).
- Li, C., Wu, W., Zhang, H., Xia, Y., Mao, S., Dong, L., Vulić, I., and Wei, F. Imagine while reasoning in space: Multimodal visualization-of-thought, 2025. URL <https://arxiv.org/abs/2501.07542>.
- Lightman, H., Kosaraju, V., Burda, Y., Edwards, H., Baker, B., Lee, T., Leike, J., Schulman, J., Sutskever, I., and Cobbe, K. Let’s verify step by step. In *The Twelfth International Conference on Learning Representations*, 2023.
- Liu, H., Li, C., Wu, Q., and Lee, Y. J. Visual instruction tuning. In *Thirty-seventh Conference on Neural Information Processing Systems*, 2023a. URL <https://openreview.net/forum?id=w0H2xGHlkw>.
- Liu, S., Zeng, Z., Ren, T., Li, F., Zhang, H., Yang, J., Jiang, Q., Li, C., Yang, J., Su, H., et al. Grounding dino: Marrying dino with grounded pre-training for open-set object detection. In *European conference on computer vision*, pp. 38–55. Springer, 2024.
- Liu, Y., Iter, D., Xu, Y., Wang, S., Xu, R., and Zhu, C. G-eval: Nlg evaluation using gpt-4 with better human alignment, 2023b. URL <https://arxiv.org/abs/2303.16634>.
- Lu, P., Bansal, H., Xia, T., Liu, J., Li, C., Hajishirzi, H., Cheng, H., Chang, K.-W., Galley, M., and Gao, J. Mathvista: Evaluating mathematical reasoning of foundation models in visual contexts. In *The Twelfth International Conference on Learning Representations*, 2024. URL <https://openreview.net/forum?id=KUNzEQMWU7>.
- Ma, T., Xie, L., Tian, Y., Yang, B., and Ye, Q. Claw-machine: Learning to fetch visual tokens for referential comprehension. In *The Thirteenth International Conference on Learning Representations*, 2025. URL <https://openreview.net/forum?id=TOtk9dTYGG>.
- Meng, F., Du, L., Liu, Z., Zhou, Z., Lu, Q., Fu, D., Han, T., Shi, B., Wang, W., He, J., Zhang, K., Luo, P., Qiao, Y., Zhang, Q., and Shao, W. Mm-eureka: Exploring the frontiers of multimodal reasoning with rule-based reinforcement learning, 2025. URL <https://arxiv.org/abs/2503.07365>.
- Muennighoff, N., Yang, Z., Shi, W., Li, X. L., Fei-Fei, L., Hajishirzi, H., Zettlemoyer, L., Liang, P., Candès, E., and Hashimoto, T. sl: Simple test-time scaling, 2025. URL <https://arxiv.org/abs/2501.19393>.
- Qwen Team. Qvq: To see the world with wisdom, December 2024. URL <https://qwenlm.github.io/blog/qvq-72b-preview/>.
- Radford, A., Kim, J. W., Hallacy, C., Ramesh, A., Goh, G., Agarwal, S., Sastry, G., Askell, A., Mishkin, P., Clark, J., Krueger, G., and Sutskever, I. Learning transferable visual models from natural language supervision, 2021. URL <https://arxiv.org/abs/2103.00020>.
- See, A., Liu, P. J., and Manning, C. D. Get to the point: Summarization with pointer-generator networks. In *Proceedings of the 55th Annual Meeting of the Association for Computational Linguistics (Volume 1: Long Papers)*, pp. 1073–1083, 2017.
- Steiner, A., Pinto, A. S., Tschannen, M., Keysers, D., Wang, X., Bitton, Y., Gritsenko, A., Minderer, M., Sherbondy, A., Long, S., et al. Paligemma 2: A family of versatile vlms for transfer. *arXiv preprint arXiv:2412.03555*, 2024.
- Sun, H.-L., Sun, Z., Peng, H., and Ye, H.-J. Mitigating visual forgetting via take-along visual conditioning for multi-modal long cot reasoning, 2025. URL <https://arxiv.org/abs/2503.13360>.
- Wang, K., Pan, J., Shi, W., Lu, Z., Ren, H., Zhou, A., Zhan, M., and Li, H. Measuring multimodal mathematical reasoning with math-vision dataset. In *The Thirty-eight Conference on Neural Information Processing Systems Datasets and Benchmarks Track*, 2024a. URL <https://openreview.net/forum?id=QWTCcxMpPA>.

- Wang, K., Pan, J., Shi, W., Lu, Z., Ren, H., Zhou, A., Zhan, M., and Li, H. Measuring multimodal mathematical reasoning with math-vision dataset. In *The Thirty-eight Conference on Neural Information Processing Systems Datasets and Benchmarks Track*, 2024b. URL <https://openreview.net/forum?id=QWTCcxMpPA>.
- Wang, P., Bai, S., Tan, S., Wang, S., Fan, Z., Bai, J., Chen, K., Liu, X., Wang, J., Ge, W., Fan, Y., Dang, K., Du, M., Ren, X., Men, R., Liu, D., Zhou, C., Zhou, J., and Lin, J. Qwen2-vl: Enhancing vision-language model’s perception of the world at any resolution, 2024c. URL <https://arxiv.org/abs/2409.12191>.
- Wang, X., Yang, Z., Feng, C., Lu, H., Li, L., Lin, C.-C., Lin, K., Huang, F., and Wang, L. Sota with less: Mcts-guided sample selection for data-efficient visual reasoning self-improvement, 2025. URL <https://arxiv.org/abs/2504.07934>.
- Wolf, T., Debut, L., Sanh, V., Chaumond, J., Delangue, C., Moi, A., Cistac, P., Rault, T., Louf, R., Funtowicz, M., Davison, J., Shleifer, S., von Platen, P., Ma, C., Jernite, Y., Plu, J., Xu, C., Scao, T. L., Gugger, S., Drame, M., Lhoest, Q., and Rush, A. M. Transformers: State-of-the-art natural language processing. In *Proceedings of the 2020 Conference on Empirical Methods in Natural Language Processing: System Demonstrations*, pp. 38–45, Online, October 2020. Association for Computational Linguistics. URL <https://www.aclweb.org/anthology/2020.emnlp-demos.6>.
- Wortsman, M., Liu, P. J., Xiao, L., Everett, K., Alemi, A., Adlam, B., Co-Reyes, J. D., Gur, I., Kumar, A., Novak, R., et al. Small-scale proxies for large-scale transformer training instabilities. *arXiv preprint arXiv:2309.14322*, 2023.
- Wu, P. and Xie, S. V\*: Guided visual search as a core mechanism in multimodal llms, 2023. URL <https://arxiv.org/abs/2312.14135>.
- Wu, Q., Yang, X., Zhou, Y., Fang, C., Song, B., Sun, X., and Ji, R. Grounded chain-of-thought for multimodal large language models, 2025. URL <https://arxiv.org/abs/2503.12799>.
- Xiao, B., Wu, H., Xu, W., Dai, X., Hu, H., Lu, Y., Zeng, M., Liu, C., and Yuan, L. Florence-2: Advancing a unified representation for a variety of vision tasks. In *Proceedings of the IEEE/CVF Conference on Computer Vision and Pattern Recognition*, pp. 4818–4829, 2024.
- Xu, G., Jin, P., Li, H., Song, Y., Sun, L., and Yuan, L. Llava-cot: Let vision language models reason step-by-step, 2025. URL <https://arxiv.org/abs/2411.10440>.
- Yang, Z., Li, L., Wang, J., Lin, K., Azarnasab, E., Ahmed, F., Liu, Z., Liu, C., Zeng, M., and Wang, L. Mm-react: Prompting chatgpt for multimodal reasoning and action. *arXiv preprint arXiv:2303.11381*, 2023.
- Yao, H., Huang, J., Wu, W., Zhang, J., Wang, Y., Liu, S., Wang, Y., Song, Y., Feng, H., Shen, L., and Tao, D. Mulberry: Empowering mllm with o1-like reasoning and reflection via collective monte carlo tree search, 2024. URL <https://arxiv.org/abs/2412.18319>.
- Zhang, J., Khayatkhoei, M., Chhikara, P., and Ilievski, F. MLLMs know where to look: Training-free perception of small visual details with multimodal LLMs. In *The Thirteenth International Conference on Learning Representations*, 2025. URL <https://openreview.net/forum?id=DgaY5mDdmT>.
- Zhang, R., Jiang, D., Zhang, Y., Lin, H., Guo, Z., Qiu, P., Zhou, A., Lu, P., Chang, K.-W., Qiao, Y., et al. Mathverse: Does your multi-modal llm truly see the diagrams in visual math problems? In *European Conference on Computer Vision*, pp. 169–186. Springer, 2024a.
- Zhang, Z., Zhang, A., Li, M., hai zhao, Karypis, G., and Smola, A. Multimodal chain-of-thought reasoning in language models. *Transactions on Machine Learning Research*, 2024b. ISSN 2835-8856. URL <https://openreview.net/forum?id=y1pPWFVfvR>.

## Overview of the Appendix

This Appendix is structured as follows:

- Section A describes implementation details and resources used in the project;
- Section B discusses limitations and future directions;
- Section C provides details of the data generation process;
- Section D reports human evaluation results validating the grounding quality of our training dataset (**v1g**) and our model (**v1**);
- Section E details pseudo-code on the visual grounding pipeline we utilized in the data generation process;
- Section F presents additional qualitative results.

### A. Implementation Details & Resources

**Training Details** All models are trained under uniform settings: a base learning rate of  $3 \times 10^{-5}$ , per-device batch size of 2, and gradient accumulation over 4 steps. We leverage DeepSpeed for distributed training across 8 NVIDIA A100 GPUs. Optimization uses AdamW with  $\beta_1 = 0.9$ ,  $\beta_2 = 0.95$ , and training is performed for 5 epochs.

**Training Duration** Our training schedule of 5 epochs follows the setup used for the original text-only reasoning trace dataset, which we extend to the grounded reasoning setup (Sun et al., 2025). Because the reasoning traces contain substantially longer token sequences than typical MLLM data, shorter training runs produced unstable behaviors such as repetition and incomplete reasoning without a final answer. In contrast, the point-and-copy behavior required relatively little data and typically saturated within the first epoch, as indicated by an early plateau in copy-token accuracy. The longer schedule therefore reflects the requirements of the inherited reasoning-trace setup rather than the needs of the pointer mechanism itself.

### B. Limitations and Future Work

This work focuses on demonstrating the effectiveness of active visual reference in structured multimodal reasoning via a simple point-and-copy mechanism. While **v1** shows strong performance in mathematical domains, several directions remain for broader applicability.

**Beyond mathematical domains.** Extending **v1** to other settings (*e.g.* such as scientific diagrams, medical images, or visual commonsense) presents new challenges in representation and supervision. These domains often lack structured reasoning traces, making data collection more difficult. Since **v1g** relies on a pretrained text-only MLLM to seed reasoning, generalizing to less structured domains will require advances in decomposition, grounding, and alignment.

**Weak supervision and reinforcement learning.** Recent work in inference-time scaling and alignment has shown the promise of reward-based learning for reasoning. Incorporating such methods into **v1** may enable more flexible and efficient visual retrieval strategies without dense supervision. We leave this exploration to future work due to current resource constraints.

### C. Data Generation Details

Figure 7 illustrates the construction pipeline for our **v1g** dataset; each stage of this pipeline is described in detail in Section 4.3. The specific prompt template used to decompose text-based reasoning paths into visual queries (as outlined in our methodology in Section 4.3) is provided in Table 5.

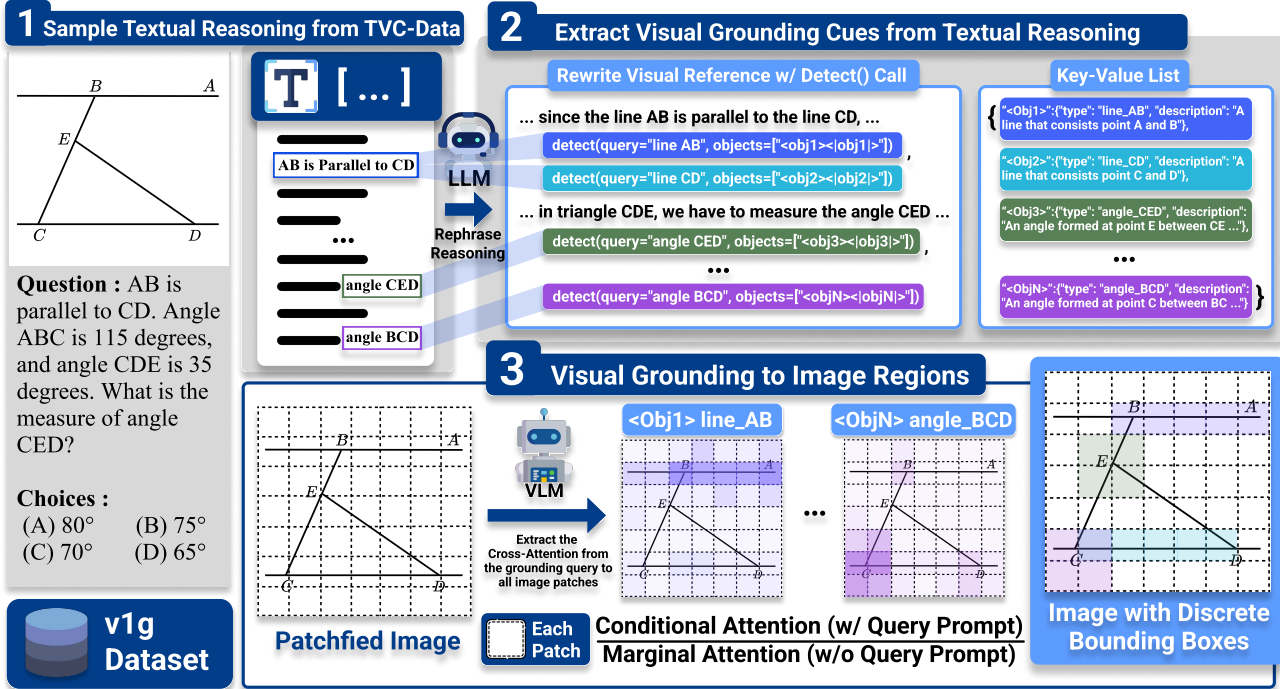


Figure 7. v1g dataset construction pipeline.

## D. Human Evaluation of Grounding Quality

### D.1. Evaluation of v1g Dataset Quality

To validate the quality of our automatically generated visual grounding annotations in the v1g dataset, we conducted a human evaluation comparing our attention-based grounding approach against GroundingDINO (Liu et al., 2024), a widely used open-set object detector.

**Methodology.** We randomly sampled 100 examples from the v1g dataset, each containing multiple bounding boxes. Three expert annotators independently evaluated each bounding box using binary classification on three criteria:

- **Correctness:** Whether the bounding box covers the intended object or region
- **Comprehensiveness:** Whether all relevant visual content is included within the box
- **Tightness:** Whether the box is well-fitted with minimal extraneous background

We report the average score across annotators, majority vote, and Fleiss’  $\kappa$  to assess inter-annotator agreement. Agreement quality follows standard interpretations: Fair (0.21–0.40), Moderate (0.41–0.60), Substantial (0.61–0.80), and Almost Perfect (0.81–1.00).

**Results.** As shown in Table 3, our attention-based grounding method substantially outperforms GroundingDINO on correctness (83.3% vs. 29.3% average score), demonstrating superior capability in localizing semantically complex and context-dependent entities such as geometric elements (e.g., “angle ABC”), chart components (e.g., “bar for Grace”), and referring expressions (e.g., “the second figure”). While GroundingDINO achieves higher inter-annotator agreement, this primarily reflects consistent failure modes rather than quality, as evidenced by its low absolute performance.

### D.2. Evaluation of v1 Pointing Accuracy

We additionally evaluated the pointing accuracy of our trained v1 model to assess how effectively it grounds visual references during inference.

Table 3. Human evaluation of v1g dataset quality.

Method	Metric	Avg	Majority	Fleiss' $\kappa$	Agreement
Attention-based (Ours)	Correctness	83.3%	87.0%	0.352	Fair
	Comprehensive.	55.0%	56.0%	0.582	Moderate
	Tightness	46.0%	44.0%	0.436	Moderate
Grounding-DINO	Correctness	29.3%	30.0%	0.711	Substantial
	Comprehensive.	47.3%	49.0%	0.906	Almost Perfect
	Tightness	19.0%	18.0%	0.675	Substantial

Table 4. Human evaluation of v1 model pointing quality.

Metric	Avg	Majority	Fleiss' $\kappa$	Agreement
Correctness	82.7%	87.0%	0.558	Moderate
Comprehensiveness	55.7%	54.0%	0.689	Substantial
Tightness	49.3%	40.0%	0.280	Fair
Appropriateness	87.7%	90.0%	0.599	Moderate

**Methodology.** Using the same evaluation protocol, we sampled 100 outputs from v1 on the MathVision dataset. Annotators evaluated whether the model’s pointed regions (copied image tokens) correctly corresponded to the referenced objects in the reasoning trace. We added an **Appropriateness** criterion to assess whether the pointing action was contextually justified.

**Results.** Table 4 demonstrates that v1 maintains high grounding quality during inference, achieving 82.7% correctness; comparable to the training data quality. The high appropriateness score (87.7%) indicates that the model learns to selectively invoke the pointing mechanism when dynamic visual reference is genuinely beneficial for reasoning.

**Discussion.** The evaluation reveals that our attention-based grounding excels at capturing semantically rich visual references that are challenging for traditional object detectors. The moderate tightness scores across both methods reflect the inherent ambiguity in defining precise boundaries for abstract concepts (e.g., "angle 2" or "the second figure"), where multiple valid interpretations exist. The consistency between training data quality and model performance suggests that v1 successfully learns robust visual grounding capabilities from our automatically generated supervision.

## E. Bounding-Box Extraction from Cross-Attention

This section provides a high-level pseudocode description of our data annotation method for deriving bounding boxes from cross-attention in Qwen-2.5-VL.

## F. Additional Qualitative Results

To further illustrate v1’s complex visual reasoning, this section provides additional qualitative examples, complementing Figure 5 from the main text. These examples highlight how v1 leverages the point-and-copy mechanism.

Figure 8 demonstrates v1 on a synthetic task (CLEVR-like) requiring object counting based on the query: “Subtract all red things, then subtract all tiny matte balls. How many objects are left?”. v1 first localizes objects using its pointer mechanism. It then sequentially reasons, identifying “red” objects before revisiting relevant items, like the “cyan sphere,” to verify the combined “tiny” and “matte” attributes through targeted attention. This process demonstrates v1’s capacity for precise attribute grounding and multi-step compositional reasoning enabled by the point-and-copy mechanism.

In Figure 9, v1 tackles a chart comprehension task: determining if the “Dark Violet” data series has the minimum area under the curve. v1 initially grounds key chart elements, using its pointer to isolate data series such as “Dark Violet,” “Medium Mint,” and “Dark Cyan.” Later in its reasoning, it proactively revisits these series, performing a comparative analysis of their visual trajectories and relative y-axis values to infer their respective areas. Such selective re-focusing showcases its ability to perform nuanced comparisons within dense visual information.

These examples further affirm that v1’s architecture, by supporting active visual reference and precise grounding via its pointing mechanism, achieves robust, interpretable, and accurate multi-step visual reasoning.

---

**Algorithm 1** Bounding-Box Extraction from Cross-Attention (High-Level)

---

**Input:** Image  $I$ , region description  $T$

**Output:** Bounding box  $b$  corresponding to  $T$

**1. Prepare multimodal input.**

Concatenate  $I$  with a static visual-grounding instruction prompt and feed it to Qwen2.5-VL.

**2. Extract attention with instruction.**

From the final decoding position, obtain the cross-attention map  $A$  over image tokens. Use a predefined set of layers (selected empirically) and average across heads.

**3. Extract baseline attention.**

Remove the object name from the prompt, feed the modified prompt with  $I$  to the model, and extract the corresponding attention map  $A'$  using the same layers and averaging.

**4. Compute attention contrast.**

Compute the contrastive relevance for each image token:  $R = A/A'$ .

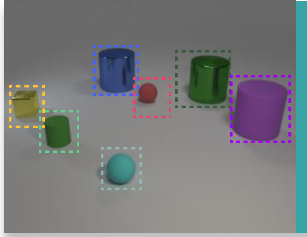
**5. Derive bounding region.**

Identify the peak region in  $R$ . Sweep over multiple candidate crop ratios; for each ratio, form a bounding region around the peak. Select the bounding box maximizing contrast sharpness between inside and outside regions. Convert the selected region to image-coordinate bounding box  $b$ .

**6. Return.**

return  $b$

---



**Question:**

Subtract all red things. Subtract all tiny matte balls. How many objects are left?

**Answer: 5**

Image-Question Pair

Let me see what objects are present. I need to identify all the objects first.

```

detect(query="yellow cube", objects=["<obj1><region>[0.00, 0.00, 0.21, 0.55]<copy_0><copy_1> ... <copy_45><copy_46></region>"])
detect(query="blue cylinder", objects=["<obj2><region>[0.29, 0.20, 0.46, 0.45]<copy_14><copy_15> ... <copy_48><copy_49></region>"])
detect(query="green cylinder", objects=["<obj3><region>[0.58, 0.20, 0.75, 0.50]<copy_17><copy_18> ... <copy_50><copy_51><copy_52></region>"])
detect(query="purple cylinder", objects=["<obj4><region>[0.75, 0.45, 0.96, 0.65]<copy_52><copy_53> ... <copy_64><copy_65></region>"])
detect(query="small green cylinder", objects=["<obj5><region>[0.12, 0.45, 0.29, 0.75]<copy_45><copy_46> ... <copy_68><copy_69></region>"])
detect(query="red sphere", objects=["<obj6><region>[0.46, 0.30, 0.54, 0.45]<copy_27><copy_38><copy_49></region>"])
detect(query="cyan sphere", objects=["<obj7><region>[0.33, 0.65, 0.46, 0.85]<copy_58><copy_59> ... <copy_81><copy_82></region>"])
    
```

The task is to subtract all red things and all tiny matte balls.

Let me consider the order: first, subtract all red things, then subtract all tiny matte balls.

Step 1: Subtract all red things. There's only one red sphere <obj6>. So, remove that.

Remaining objects: 1. Yellow cube <obj1> 2. Blue cylinder <obj2> 3. Green cylinder <obj3> 4. Purple cylinder <obj4> 5. Small green cylinder <obj5> 6. Cyan sphere <obj7>

Step 2: Subtract all tiny matte balls. Assuming the cyan sphere <obj7> is matte, it should be removed. So, remove the cyan sphere <obj7>.

Remaining objects: 1. Yellow cube <obj1> 2. Blue cylinder <obj2> 3. Green cylinder <obj3> 4. Purple cylinder <obj4> 5. Small green cylinder <obj5>

That's five objects.

Wait, but the problem might be considering only the red sphere <obj6> as matte, and the cyan sphere <obj7> is also matte. But since it's not specified, I'll assume both are matte.

Alternatively, perhaps "tiny matte balls" refer only to the cyan sphere <obj7>, and the red sphere <obj6> is not considered a "ball" or something. But the problem mentions "tiny matte balls," and both spheres are small and matte, so probably both are considered tiny matte balls. Therefore, after subtracting the red sphere <obj6> and the cyan sphere <obj7>, we're left with five objects: yellow cube <obj1>, blue cylinder <obj2>, green cylinder <obj3>, purple cylinder <obj4>, and small green cylinder <obj5>.

But wait, the user's message seems to indicate there are six objects initially, but lists seven, which is confusing. Maybe there's a mistake in counting. Alternatively, perhaps the small green cylinder <obj5> is not present, and there are only six objects: Yellow cube <obj1>, Blue cylinder <obj2>, Red sphere <obj6>, Green cylinder <obj3>, Purple cylinder <obj4>, Cyan sphere <obj7>

In this case, after subtracting the red sphere <obj6> and the cyan sphere <obj7><region>[0.33, 0.65, 0.46, 0.85]<copy\_58><copy\_59> ... <copy\_81><copy\_82></region>, we're left with four objects: yellow cube <obj1>, blue cylinder <obj2>, green cylinder <obj3>, purple cylinder <obj4>.

But the user mentioned six objects, including the small green cylinder <obj5>, so I'll stick with that.

Alternatively, maybe the small green cylinder <obj5> is separate from the green cylinder <obj3>, making it seven distinct objects. Regardless, the key is to subtract the red sphere <obj6> and the cyan sphere <obj7>, assuming both are matte.

So, final answer should be 5 or 4, depending on whether the small green cylinder is considered separate or part of the green cylinder. But since the user specified seven objects, including small green cylinder <obj5>, the answer should be 5. **Final Answer**  $\boxed{5}$

Figure 8. Qualitative example of v1 tackling an attribute-based counting task in a synthetic domain.



**Question:**

Does Dark Violet have the minimum area under the curve?

**Choices:**

(A) yes (B) no

Image-Question Pair

Alright, I've got this graph to analyze. First, I need to detect the graph.

detect(query="the graph", objects=["<obj1><region>[0.00, 0.00, 1.00, 1.00]<copy\_0><copy\_1> ... <copy\_310><copy\_311></region>"])

There are five different data series here, each represented by a different color: Dark Violet, Hot Pink, Medium Mint, Dark Cyan, and Yellow Green. I need to detect each data series.

detect(query="Dark Violet data series", objects=["<obj2><region>[0.12, 0.77, 0.79, 0.93]<copy\_219><copy\_220> ... <copy\_306><copy\_307></region>"])

detect(query="Hot Pink data series", objects=["<obj3><region>[0.21, 0.23, 0.58, 0.46]<copy\_52><copy\_53> ... <copy\_157><copy\_158></region>"])

detect(query="Medium Mint data series", objects=["<obj4><region>[0.12, 0.54, 0.54, 0.85]<copy\_147><copy\_148> ... <copy\_276><copy\_277></region>"])

detect(query="Dark Cyan data series", objects=["<obj5><region>[0.25, 0.15, 0.54, 0.38]<copy\_30><copy\_31> ... <copy\_108><copy\_109></region>"])

detect(query="Yellow Green data series", objects=["<obj6><region>[0.08, 0.07, 0.79, 0.77]<copy\_1><copy\_2> ... <copy\_258><copy\_259></region>"])

The y-axis is labeled "label" and ranges from 86 to 98, and the x-axis is numbered from 0 to 100. I need to detect the y-axis and x-axis.

detect(query="y-axis", objects=["<obj7><region>[0.00, 0.30, 0.04, 0.62]<copy\_72><copy\_73> ... <copy\_192><copy\_193></region>"])

detect(query="x-axis", objects=["<obj8><region>[0.33, 0.84, 0.50, 1.00]<copy\_247><copy\_248> ... <copy\_298><copy\_299></region>"])

Looking at the plot <obj1>, I can see that each of these has points scattered across the graph area.

Starting with Dark Violet <obj2>, which is purple. It seems like there are several purple points clustered towards the lower part of the graph <obj1>, around the 86 mark on the y-axis <obj7>. They don't seem to vary much in value, suggesting that this might be a relatively flat line or very little change over the x-axis <obj8> range.

Hot Pink <obj3>, which is light pink, shows a more dynamic pattern. The points start high around 98 and seem to decrease gradually as the x-axis <obj8> progresses. There might be some fluctuation, but overall, there's a downward trend.

Medium Mint <obj4>, the light greenish-blue, starts low around 86 and increases steadily, possibly following a linear pattern. By the end, it reaches up to about 92 or 93.

Dark Cyan <obj5>, the dark blue-green, appears to be quite variable. It starts around 96 and fluctuates up and down, sometimes dipping below 94 and rising above 96.

Yellow Green <obj6>, the yellowish-green, also shows variability, starting around 96 and fluctuating between about 92 and 96.

...

From the description, it seems that Dark Violet <obj2> is consistently around 86, with minimal variation. Comparatively, Medium Mint <obj4><region>[0.12, 0.54, 0.54, 0.85]<copy\_147><copy\_148> ... <copy\_276><copy\_277></region> starts at 86 and increases to about 92 or 93, so its average would be higher than Dark Violet's <obj2>. Similarly, Dark Cyan <obj5><region>[0.25, 0.15, 0.54, 0.38]<copy\_30><copy\_31> ... <copy\_258><copy\_259></region> have higher y-values, so their areas would be larger.

Hot Pink <obj3><region>[0.21, 0.23, 0.58, 0.46]<copy\_52><copy\_53> ... <copy\_157><copy\_158></region> starts high and decreases, but even at its lowest, it's around 90, which is still higher than Dark Violet's <obj2> average.

Therefore, based on this analysis, Dark Violet <obj2> indeed has the smallest area under the curve.

So, the answer should be (A) yes. **\*\*Final Answer\*\***[ \boxed{A} \]

Figure 9. Qualitative example of v1 performing comparative reasoning on a chart comprehension task.

Prompt for data generation

You are given text-only reasoning for visual question answering.

Your task is to convert this text-only reasoning into visually grounded reasoning.

### STEP-BY-STEP INSTRUCTION

Please follow these instructions step-by-step, imitating human visual reasoning behavior by:

- 1) Start from the beginning of the reasoning and read EACH sentence.
- 2) When you think you'd better look at the object or region, use the detect() function.
- 3) Format: 'detect(query="visual item that you want to find", objects=["<obj#>"])'
- 4) After detection, reference the visual element with '<obj#>' tags every time you need to look at it again immediately after mentioning the item.
- 5) Use NEW object numbers ('<obj1>', '<obj2>', '<obj3>'...) for EACH new detection.

### EXAMPLE:

Original text:

"Looking at the graph, I can see the function reaches its maximum at  $x = 3$ ."

Corrected:

""

To answer the question, I need to look the graph.

detect(query="function graph", objects=["<obj1>"])

Looking at the graph <obj1>, I can see the function reaches its maximum at  $x = 3$ .

""

Later reference:

You can skip the <obj#> tag when you think you do not need to look it again.

""

The slope of the function becomes zero at this point on the graph.

""

### KEY REQUIREMENTS:

- Every item in lists MUST have its own 'detect()' statement
- Put 'detect()' statements on their own lines
- NEVER skip any visual element mentioned in the reasoning
- Start object numbering at 'obj1' and increase by 1 for each new object

### <OBJ#> REQUIREMENTS

- Visual element should be concrete, distinct, and explicit. Later you will localize the element based on the detect(). So make sure that the element not confusing.
- Use separate tags for each object (write "between the bus <obj1> and the car <obj2>" not "between <obj1 and obj2>").
- GOOD grounding: "I need to analyze this problem. detect(query="triangle", objects=["<obj1>"]) The triangle <obj1> has a right angle at vertex S."
- BAD grounding: "detect(query="triangle and rectangular", objects=["<obj1>"]) in the diagram, there are the triangle and rectangular has a right angle." (referring to non-atomic element)
- BAD grounding: "detect(query="region", objects=["<obj1>"]) The triangle <obj1> has a right angle." (referring to ambiguous element)

After completing the reasoning, list all objects detected:

```
{
  "obj1": {"type": "function_graph",
  "description": "Graph of a function with maximum at  $x = 3$ "},
  "obj2": {"type": "next_item",
  "description": "Description of next item"}
```

}

- We will localize the element with the open-world detector based on the description, so make sure to include well-described full self-contained description enough to uniquely identify the object.

### FINAL FORMAT:

```
{
"reasoning": "Your fully visually-grounded reasoning text",
"obj_list": "Your JSON object list"
}
```

Now, strictly following the instruction and the example, please provide the object list and visually grounded reasoning for the following prompt and reasoning:

### Example

Original Conversation

HUMAN:

[few\_shot\_question]

GPT:

[few\_shot\_answer]

### Visually Grounded Reasoning

GPT:

[few\_shot\_reasoning]

### Object List:

[few\_shot\_objects]

Now, given the conversation, please convert GPT's text-only reasoning into visually grounded reasoning

Original Conversation:

HUMAN:

[question]

GPT:

[answer]

### Visually Grounded Reasoning:

Table 5. Prompt used for converting textual reasoning to grounded reasoning annotations in **v1g** data generation process.